Photoassociation spectroscopy in Penning ionization reactions at sub-Kelvin temperatures

Wojciech Skomorowski,[1] Yuval Shagam,[2] Edvardas Narevicius,[2] and Christiane P. Koch[1]

[1] *Theoretische Physik, Universität Kassel, Heinrich-Plett-Straße 40, 34132 Kassel, Germany*

[2] *Department of Chemical Physics, Weizmann Institute of Science, Rehovot 76100, Israel*

(Dated: January 5, 2016)

Abstract

Penning ionization reactions in merged beams with precisely controlled collision energies have been shown to accurately probe quantum mechanical effects in reactive collisions. A complete microscopic understanding of the reaction is, however, faced with two major challenges—the highly excited character of the reaction's entrance channel and the limited precision of even the best state-of-the-art *ab initio* potential energy surfaces. Here, we suggest photoassociation spectroscopy as a tool to identify the character of orbiting resonances in the entrance channel and probe the ionization width as a function of inter-particle separation. We introduce the basic concept and discuss the general conditions under which this type of spectroscopy will be successful.

I. INTRODUCTION

Understanding chemical reaction dynamics in a microscopic perspective from first principles has been a long standing goal in physical chemistry. Over many decades, molecular beams have been the prime tool to study gas phase reactions. Controlling the beams with electric or magnetic fields has recently rejuvenated this field [1–3]. In particular, merging two beams with a magnetic field [4–9] has allowed for unprecedented control over the collision energy, both in terms of accessible range and precision. Studying Penning ionization reactions with this technique comes with the additional advantage of nearly unit efficiency in detecting the ionic reaction products. This has allowed for observing orbiting resonances at sub-Kelvin temperatures [4] including an isotope effect [5] and elucidating the role of internal rotation for the reaction [9]. However, a complete microscopic understanding of the reaction dynamics requires high-level *ab initio* theory in addition to precise experimental data. While the entrance channel of the reaction can be described with reasonable accuracy [10], a full model of Penning ionization reactions is faced with two major challenges. First, since it necessarily involves metastable states, the entrance channel is a highly excited electronic state, which is embedded in a continuum of ionized states. The corresponding electronic wave function does not belong to the space of square integrable functions and thus cannot be correctly described by standard electronic structure methods, designed for the description of bound states. The difficulty of coupling to a continuum of ionized states can be circumvented by replacement with an imaginary potential, defined within the Fano-Feshbach formalism for an isolated resonance [11, 12]. In this approach, a projection operator is introduced, which allows to partition the total Hilbert space into discrete and continuum parts. The imaginary potential is obtained from the coupling matrix elements between wave functions in the two subspaces. However, choice and construction of the Feshbach projection operator are highly nontrivial. Second, even for diatomics, the best, currently available potential energy curves are not sufficiently accurate to correctly predict the scattering length and thus exact position and character of orbiting resonances [13].

Here, we suggest photoassociation spectroscopy of Penning ionization reactions to address these two issues. Photoassociation refers to the formation of a chemical bond upon laser excitation [14, 15]. In standard photoassociation spectroscopy, the laser excites two colliding ground state atoms to an electronically excited state. Detuning the laser frequency from

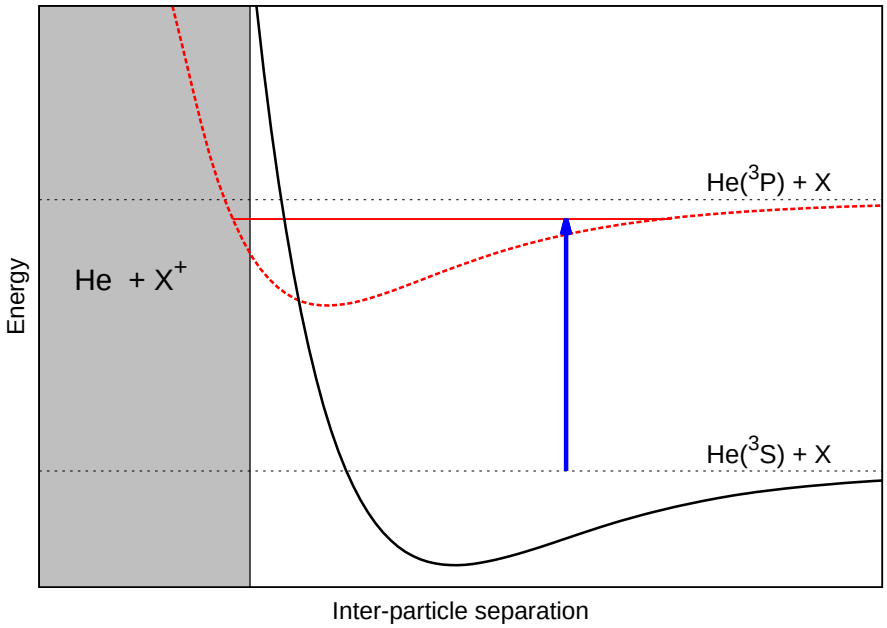

FIG. 1: Photoassociation spectroscopy in Penning ionization. The laser, indicated by the blue arrow, excites a scattering pair colliding with collision energy E in the He(^3S)+X state into a bound rovibrational level in the potential energy curve dissociating into He(^3P)+X. The grey shaded area at short inter-particle separations indicates the region where the probability for Penning ionization is unity. If the bound level extends into this region, ionization will happen faster than in the entrance channel, i.e., photoassociation will be obserevd in terms of an increased ionization rate.

the atomic excitation energy probes molecular levels below the excited state dissociation threshold [14, 15]. Photoassociation rates are limited by the amplitude of collision wavefunctions at the Condon radius, i.e., the inter-particle separation where the laser frequency matches the energy difference between ground and excited potential energy surface [16]. At sub-Kelvin temperatures, only few partial waves contribute to the collision and, due to the rotational barrier and quantum reflection, their wavefunctions have little amplitude at short inter-particle separations. Photoassociation is thus most effecient at intermediate and large separations [17]. This implies excitation into weakly bound levels just below the dissociation threshold.

When applied to a collision complex undergoing a Penning ionization reaction, the electronic ground state as entrance channel is replaced by a metastable one, see Fig. 1. Such a configuration of electronic states can also be used to produce metastable diatomic helium molecules via photoassociation [18]. While in that case, the giant bond length of the

helium dimer precludes Penning ionization, here we consider interactions where the particles approach each other close enough to Penning ionize. As specific example, we consider photoassociation in the Penning ionization of metastable helium and argon. However, our considerations hold also when argon is replaced by a different ground state scattering partner X. Penning ionization in collisions between He(^3S) and Ar was extensively studies in the past, see Ref. [19] and references therein; the most recent state-of-the-art experimental investigation used velocity controlled merged beams [4]. As indicated by the blue arrow in Fig. 1, the laser is taken to be red-detuned with respect to the $^3P \leftarrow {}^3S$ line of helium, which is a dipole-allowed transition,

$$\mathrm{He}(^3S) + \mathrm{Ar} \xrightarrow{h\nu} \mathrm{He}(^3P)\mathrm{Ar}\,.$$

Excitation then happens into bound levels below the He(^3P)+Ar threshold. Since the excited state potential energy curve extends to shorter inter-particle separation, where the probability for Penning ionization is significantly increased, the reaction rate is larger than in the entrance channel. Such a configuration of potential energy curves has recently been reported for Penning ionization in He(^3P)+H_2 compared to that in He(^3S)+H_2, resulting in orders of magnitude larger reaction rates [9]. Photoassociation should thus be measurable by an enhancement of the Penning ionization rate. However, observation of the bound levels is possible only, if the Penning ionization reaction is not too fast. More quantitatively, the inverse lifetime of the bound levels due to Penning ionization needs to be smaller than the level spacing. We will discuss the prospects for photoassociation spectroscopy for the example of the Penning ionization of metastable helium and argon, based on a first principles model.

The remainder of the paper is organized as follows: We introduce our model and the computational details in Section II and present our results in Section III. In particular, we discuss prospects to use photoassociation spectroscopy as a means to unequivocally identify the rotational quantum number of orbiting resonances and as a tool to map out the imaginary potential governing the ionization probability. We conclude in Section IV.

II. MODEL AND COMPUTATIONAL DETAILS

The interaction between two particles undergoing a Penning ionization reaction can be modeled be means of a complex potential [19],

$$W(R) = V(R) + \frac{i}{2}\,\Gamma(R)\,, \tag{1}$$

where R denotes inter-particle separation. $V(R)$ is the real part of the potential and $\Gamma(R)$ its width, also called imaginary or optical potential. In a semi-classical picture, $V(R)$ governs the collisional dynamics of the interacting species while $\Gamma(R)$ reflects the probability for Penning ionization as a function of inter-particle distance. Both $V(R)$ and $\Gamma(R)$ depend on the electronic state, on which the interaction takes place.

In our model of Penning ionization of metastable helium and argon, three non-relativistic electronic states are relevant: $(1)^3\Sigma^+$, asymptotically dissociating into He(^3S) + Ar atoms, and $(2)^3\Sigma^+$ and $^3\Pi$, dissociating into He(^3P) + Ar atoms. For each electronic state, $V(R)$ is obtained from *ab initio* calculations. The potential of the $(1)^3\Sigma^+$ state is taken from Ref. [10]. For the states resulting from the interaction of argon with He(^3P), we have calculated the relevant potential energy curves by using the spin-restricted open-shell coupled cluster method restricted to single, double, and noniterative triple excitations [RCCSD(T)]. In the initial restricted open-shell Hartree-Fock (ROHF) calculations, we have alternated the occupied orbitals in order to force convergence of the ROHF wave function to the desired excited electronic state. A similar approach was successfully used to describe the interaction between He($^3S, ^3P$) and H_2 [9, 10]. Here, we have employed a doubly augmented d-aug-cc-pVQZ basis set for the helium atom and a singly augmented aug-cc-pVQZ basis set for the argon atom [20]. The electronic structure calculations were performed with the MOLPRO suite of codes [21]. The long-range part of $V(R)$, for $R > 20$ bohr was taken in its asymptotic form, C_6/R^6 accounting only for the leading order term, and fixing the van der Waals C_6 coefficients to 214.1 a.u. for the $(1)^3\Sigma^+$ state [10], 369.2 a.u. for the $(2)^3\Sigma^+$ state, and 201.9 for the $^3\Pi$ state. To calculate the last two C_6 coefficients, the polarizability for He(^3P) was constructed from the sum-over-states expression as described in Ref. [9].

For the imaginary part, we have employed the functional form of $\Gamma(R)$ from Ref. [22],

$$\Gamma(R) = Ae^{-\alpha R} + Be^{-\beta R}\,, \tag{2}$$

where the original values of the parameters, $A = 896\,\mathrm{eV}$, $B = 0.0043\,\mathrm{meV}$, $\alpha = 4.08\,\mathrm{\AA}^{-1}$ and

$\beta = 0.28\,\text{Å}^{-1}$, were obtained by a fitting procedure to reproduce the Penning ionization cross sections for collisions between He(^3S) and Ar at thermal energies [22]. We have assumed $\Gamma(R)$ to be identical for all relevant electronic states. This assumption can be justified on the grounds of recent results for He(^3S,^3P) + H_2 [9], where calculations have shown $\Gamma(R)$ to be almost the same for He(^3S) + H_2 and He(^3P) + H_2.

The Hamiltonian for the nuclear motion in each electronic state n takes the following form:

$$\widehat{H}_n = \frac{1}{2\mu}\frac{\partial^2}{\partial R^2} + \frac{l(l+1)}{2\mu R^2} + V_n(R) + \frac{i}{2}\,\Gamma(R) \tag{3}$$

with μ denoting the reduced mass, and l the rotational quantum number. In the rotational kinetic energy, we have neglected the spin-rotational coupling and nonadiabatic coupling between $^3\Sigma$ and $^3\Pi$ states. These simplifications are justified since we are mostly interested in collision energies of the order of 1 Kelvin and relatively high partial waves, $l \sim 7$, where the rotational Hamiltonian is dominated by the $l(l+1)$ term, so l is a good quantum number. Diagonalization of this Hamiltonian for each n and l gives the bound vibrational levels and continuum states. The presence of the optical potential implies complex eigenvalues, $W_{v,l} = E_{v,l} + i/2\ \Gamma^p_{v,l}$ where $E_{v,l}$ denotes the position of the resonance and $\Gamma^p_{v,l}$ is the corresponding width due to Penning ionization process.

Photoassociation rate coefficients K_{PA} for collision energies E and a laser frequency ω are obtained from the standard expression [23, 24],

$$K_{PA}(E,\omega) = \frac{\pi\hbar}{\mu k}\sum_l (2l+1)\sum_{v',l'} |S_{v',l'}(E,\omega,l)|^2\,, \tag{4}$$

where $k = \sqrt{2\mu E/\hbar^2}$, adapted to Penning ionization. The transition probability $|S_{v',l'}(E,\omega,l)|^2$ for photoassociation from a continuum state with energy E just above the He(^3S)+Ar asymptote into a bound level with quantum numbers v', l' just below the dissociation limit He(^3P)+Ar reads

$$|S_{v',l'}(E,\omega,l)|^2 = \frac{\Gamma^s_{v',l'}(E,l)\cdot\Gamma^d_{v',l'}}{(E-\Delta_{v',l'})^2 + 1/4[\Gamma^s_{v',l'}(E,l)+\Gamma^d_{v',l'}]^2}\,, \tag{5}$$

where $\Gamma^s_{v',l'}(E,l)$ is the stimulated emission rate, $\Gamma^d_{v',l'}$ the total decay rate, and $\Delta_{v',l'} = E_{v',l'} - \hbar\omega$ the detuning of the laser frequency from the vibrational level. The total decay rate $\Gamma^d_{v',l'}$ is the sum of the natural radiative width $\Gamma^n_{v',l'}$ and the Penning ionization width $\Gamma^p_{v',l'}$. At low laser intensity I, the stimulated emission rate $\Gamma^s_{v',l'}(E,l)$ is given by Fermi's

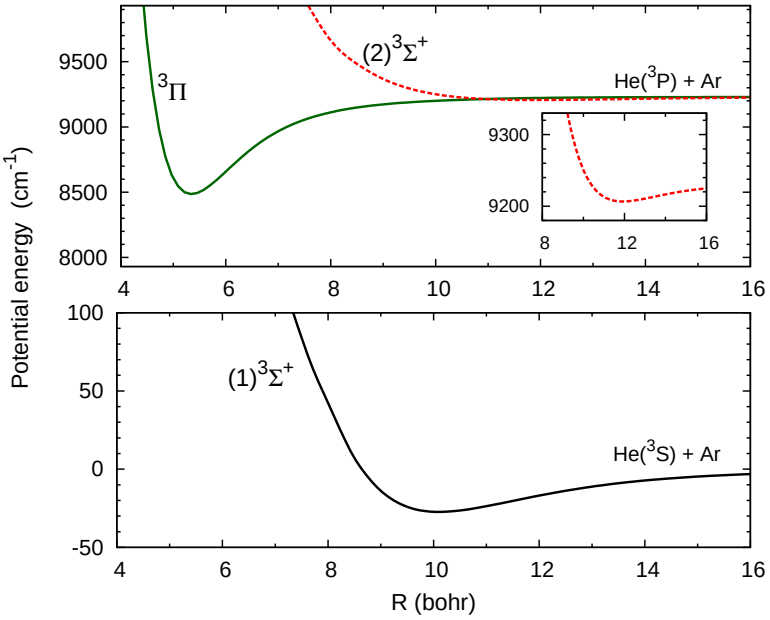

FIG. 2: Potential energy curves for the $(1)^3\Sigma^+$, $(2)^3\Sigma^+$ and $^3\Pi$ electronic states. Zero interaction energy is fixed at the He(^3S) + Ar atomic asymptote.

golden rule,

$$\Gamma^s_{v',l'}(E,l) = \frac{4\pi^2 I}{4\pi\epsilon_0 c}(2l'+1)H_{l'}|\langle\psi_{E,l}(R)|d(R)|\psi_{v',l'}\rangle|^2\,, \tag{6}$$

where $H_{l'}$ is the Höln-London factor equal to $(l'+1)/(2l'+1)$ for $l' = l-1$, to $1/(2l'+1)$ for $l = l'$, and to $l'/(2l'+1)$ for $l' = l+1$. $\psi_{E,l}(R)$ denotes the continuum wave function for energy E and partial wave l, obtained from diagonalization of the Hamiltonian for the $(1)^3\Sigma^+$ state with a very large grid, while $\psi_{v',l'}(R)$ is the bound state wave function of either the $(1)^3\Sigma^+$ or $^3\Pi$ electronic state. The molecular transition dipole moments $d(R)$ from $(1)^3\Sigma^+$ to $(2)^3\Sigma^+$ and from $(1)^3\Sigma^+$ to $^3\Pi$ electronic states were assumed to be constant and equal to the atomic transition dipole moment $^3S \leftarrow {}^3P$ in He, which is 2.53 a.u. Similarly, a constant transition dipole moment d was assumed in the calculations of the natural radiative widths $\Gamma^n_{v',l'}$. We have not performed any thermal averaging to calculate $K_{PA}(E)$ since the experimental conditions with merged beams allow for probing a particular collision energy with essentially no thermal broadening. In all photoassociation calculations we have assumed a laser intensity of 1 W/cm^2.

III. RESULTS

Figure 2 presents the three potential energy curves $V(R)$ of the helium-argon collision complex relevant for photoassociation in Penning ionization. Both the $(1)^3\Sigma^+$ and $(2)^3\Sigma^+$ states are rather shallow with their minima found at relatively large interatomic distances. More precisely, the $(1)^3\Sigma^+$ state has a well depth of $27.3\,\mathrm{cm}^{-1}$ with its equilibrium distance equal to 10.09 bohr, while the $(2)^3\Sigma^+$ state has its minimum of $24.3\,\mathrm{cm}^{-1}$ at 11.92 bohr. A qualitative difference is found for the potential energy curve of the $^3\Pi$ state, which has a predicted minimum of $745\,\mathrm{cm}^{-1}$ at 5.34 bohr. This pattern of the electronic states, with weakly bound Σ states and a strongly interacting Π state is fully analogous with the previously reported interaction potentials for He(^3S,^3P) colliding with H_2 molecules [9] or other similar systems where a single-valence atom interacts with closed-shell species, such as Li(^2S,^2P) + H_2 [25].

The entrance channel for photoassociation spectroscopy of the Penning ionization reaction is the $(1)^3\Sigma^+$ state, resulting from the interaction between metastable He(^3S) and ground-state Ar atoms. We consider a detuning of the photoassociation laser with respect to the $^3P \leftarrow {}^3S$ helium atomic line, so the targeted bound levels belong to either the $(2)^3\Sigma^+$ or the $^3\Pi$ electronic states. In our model, we neglect any nonadiabatic (spin-rotation or spin-orbit) couplings between the $(2)^3\Sigma^+$ and $^3\Pi$ states. These couplings should be important only for ultralow collisional energies and for the most weakly bound levels, where the $(2)^3\Sigma^+$ and $^3\Pi$ states are nearly degenerate. For more deeply bound levels and for sub-Kelvin or higher collision energies, the contributions from any nonadiabatic coupling would be of the order or smaller than the accuracy of the electronic potentials. Thus we can safely neglect them without compromising the essential features of our model.

Low-energy collisions between He(^3S) and Ar are characterized by several shape resonances, as recently demonstrated in an experiment with merged beams [4]. The lowest two resonances are located at approximately 0.23 Kelvin and 1.10 Kelvin. The positions of these shape resonances are comparatively well reproduced by our model—they occur at collisional energies of 0.25 Kelvin (partial wave $l = 3$) and 0.91 Kelvin (partial wave $l = 7$). Photoassociation at energies corresponding to a shape resonance is highly efficient [26]: The enhanced probability for transitions from a scattering state to a bound level is due to a largely increased amplitude of resonance wave functions. In other words, for an orbiting resonance,

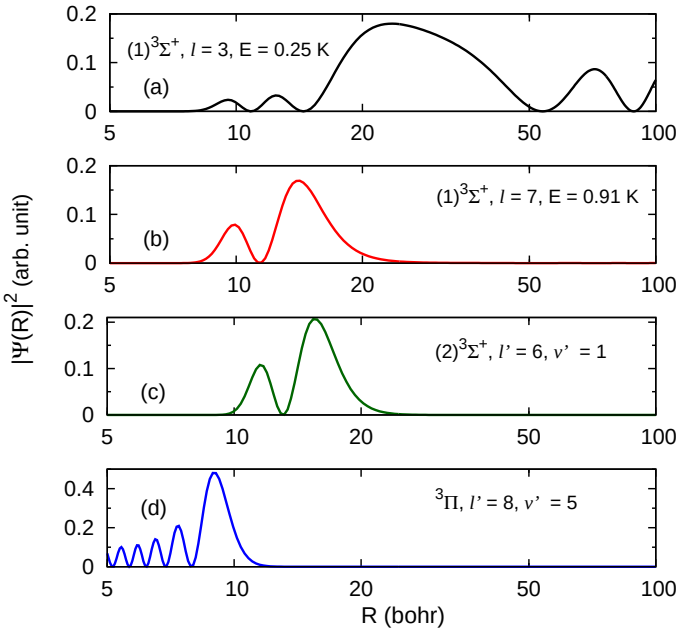

FIG. 3: (a), (b) Wave functions for two considered shape resonances in $(1)^3\Sigma^+$ state. (c), (d) Wave functions for bound levels in $(2)^3\Sigma^+$ and $^3\Pi$ electronic states particularly suited for photoassociation starting from the $l = 7$ shape resonance.

amplitude becomes trapped at short inter-particle separations, inside the rotational barrier, leading to larger transition matrix elements in photoassociation. To take advantage of this enhancement, we focus on photoassociation at collisional energies matching the theoretical positions of the lowest shape resonances, i.e., 0.25 Kelvin and 0.91 Kelvin. Somewhat inexpectedly, the nature of these two shape resonances is quite different. This is illustrated by the two upper panels of Fig. 3, showing the wave functions of these resonances. The energy of the $l = 3$ resonance is slightly above the maximum of the centrifugal barrier which is equal to 0.23 Kelvin. As a result, the wave function is fairly diffuse with only little enhancement of pair density at short inter-particle distances. In contrast, the nature of the $l = 7$ shape resonance [Fig.3(b)] is very different. It is energetically located deeply inside the well created by the centrifugal barrier. Thus the amplitude of its wave function is enhanced at short inter-particle separations, resembling at these distances the wave function of a typical bound level.

Photoassociation rates for levels in the $(1)^3\Sigma^+$ and $^3\Pi$ electronic states are obtained separately from single-channel calculations since we neglect nonadiabatic couplings. Figure 4 presents the spectrum for photoassociation into the $(2)^3\Sigma^+$ state at a collision energy of

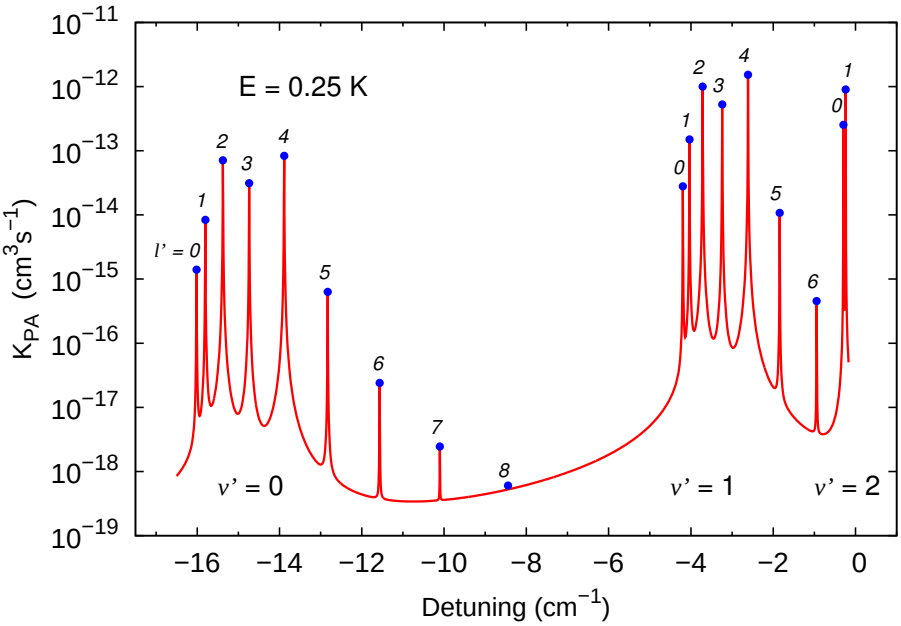

FIG. 4: Photoassociation rates as a function of laser detuning from the He $^3S \rightarrow ^3P$ atomic line for rovibrational levels of the $(2)^3\Sigma^+$ state at a collision energy of 0.25 Kelvin and a laser intensity of 1 W/cm^2. The vibrational and rotational quantum numbers are indicated for each peak. The peaks for $l' = 2, 3, 4$ are enhanced due to the $l = 3$ shape resonance as initial state at 0.25 K, whereas for all other peaks photoassociation starts from regular scattering states.

0.25 Kelvin. A rotational progression for three vibrational levels is clearly visible. Note that our potential energy curves are not sufficiently accurate to predict the exact detunings of these peaks. Refinement of the potentials based on spectroscopic information would be required to this end. However, the spacing between rotational and vibrational levels can be predicted correctly.

The highest rates in Fig. 4 occur for $2 \leq l' \leq 4$, i.e., for bound levels which are directly accessible from the $l = 3$ shape resonance. However, the observed enhancement of the rates compared to the other levels is one order of magnitude at most. This relatively minor resonance effect is easily explained by the above-the-barrier character of this shape resonance, and the corresponding diffuse nature of its wavefunction, cf. Fig. 3(a). The widths of the photoassociation lines range from 30 MHz (for $v' = 2$) up to 160 MHz (for $v' = 0$), and are almost purely determined by the Penning ionization contributions $\Gamma^p_{v',l'}$, since the width due to spontaneous radiative emission $\Gamma^n_{v',l'}$ is only of the order of 1 MHz. Increase of the peak width with binding energy is readily explained by the stronger localization of the bound level

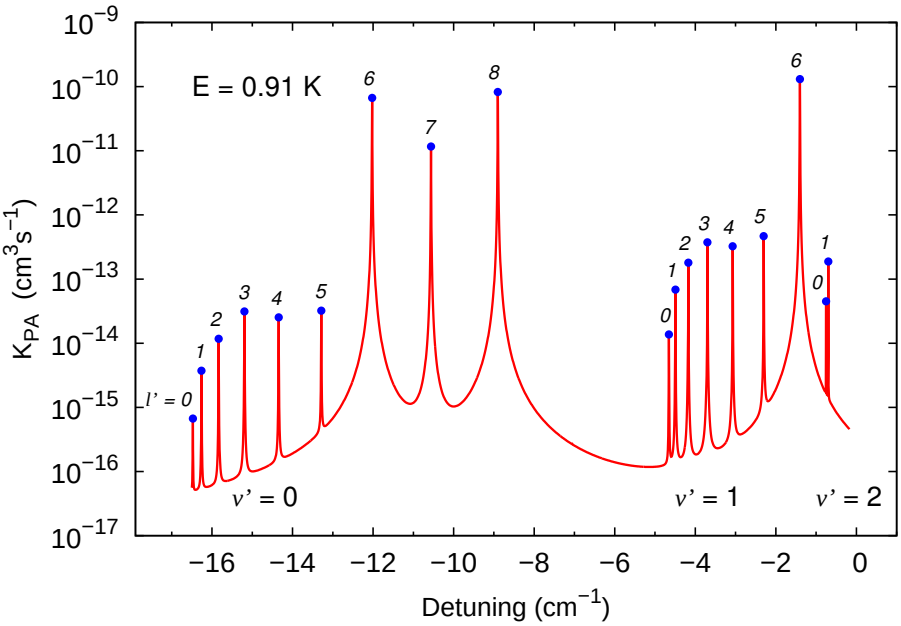

FIG. 5: Photoassociation rates as a function of laser detuning from the He $^3S \rightarrow ^3P$ atomic line for rovibrational levels of the $(2)^3\Sigma^+$ state at a collision energy of 0.91 Kelvin and a laser intensity of 1 W/cm^2. The vibrational and rotational quantum numbers are indicated for each peak. The peaks for $l' = 6, 7, 8$ are enhanced due to the $l = 7$ shape resonance as initial state at 0.91 K, whereas for all other peaks photoassociation starts from regular scattering states.

amplitude at shorter inter-particle separation together with the exponential increase of the ionization probability with decreasing inter-particle separation, cf. Eq. (2). More generally, this also explains why the bound levels ionize faster than scattering states, leading to an observable signature of photoassociation in the Penning ionization reaction.

The photoassociation spectrum for bound levels in the $(2)^3\Sigma^+$ state at a collision energy of 0.91 Kelvin is presented in Fig. 5. Here, strongly enhanced peaks are observed at detunings matching the rovibational levels with $6 \leq l' \leq 8$. These levels can be directly accessed from the $l = 7$ shape resonance at 0.91 Kelvin. The enhancement due to the shape resonance is nearly three orders of magnitude, reaching a peak rate of 10^{-10} cm^3/s for the assumed laser intensity of $I = 1$ W/cm^2, much more than in the previous case of the $l = 3$ resonance. This strong enhancement is easily rationalized by comparing the wave functions for the $l = 7$ shape resonance and the $l' = 6$, $(2)^3\Sigma^+$ bound level, shown in panels (b) and (c) of Fig. 3: The very good overlap between these wave functions leads to the predicted large photoassociation rate.

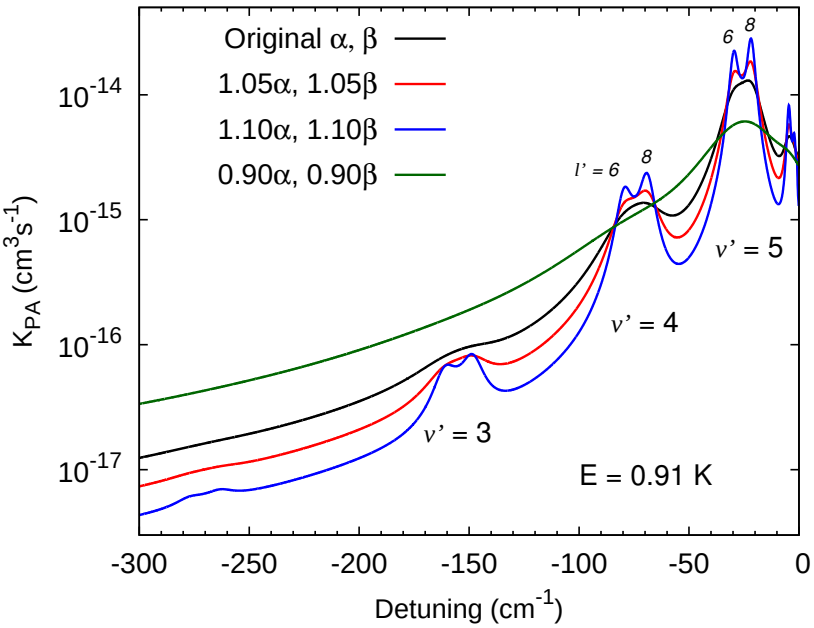

FIG. 6: Photoassociation rates as a function of laser detuning from the He $^3S \rightarrow ^3P$ atomic line for rovibrational levels of the $^3\Pi$ state at a collision energy of 0.91 Kelvin and a laser intensity of 1 W/cm^2. The vibrational and rotational quantum numbers are indicated for each peak. α and β are the parameters of the optical potential, Eq. (2), with the original values taken from Ref. [22].

Overall, Figs. 4 and 5 predict, for levels in the $(2)^3\Sigma^+$ electronic state, photoassociation spectra with a well resolved rotational-vibrational structure. Penning ionization broadens the peaks compared to the natural linewidth. However, this broadening is significantly smaller than the spacing between the lines. Thus, photoassociation spectroscopy is expected to be feasible with high resolution and can be used, for example, to determine the rotational quantum number of the shape resonance that serves as starting point. The basic feature of the potential energy curve which allows for this prediction of well-resolved photoassociation lines is a potential well at comparatively large inter-particle separation where the probability for Penning ionization is not very large.

Finally, we consider photoassociation into the $^3\Pi$ state. We focus only on a collision energy of 0.91 Kelvin, where the sharpest resonance effect and thus the clearest signal is expected. The photoassociation spectrum, obtained with the original parameters of the imaginary potential, α and β in Eq. (2), taken from Ref. [22], is presented by the black curve in Fig. 6. In contrast to the $(2)^3\Sigma^+$ state, the rovibrational structure of the spectrum has almost disappeared. For bound levels in the $^3\Pi$ state, the Penning ionization widths

are in the range from $1\,\mathrm{cm}^{-1}$ or $30\,\mathrm{GHz}$ (for the weakly bound $v' = 7$ level) up to $60\,\mathrm{cm}^{-1}$ (for the most deeply bound $v' = 0$ level). These large widths, comparable to the spacings between the rovibrational levels, do not allow to resolve individual lines in the spectrum, in particular for larger detunings, i.e., larger binding energies. This raises the question how the strength of the imaginary potential, or more precisely whether and how the parameters α and β in Eq. (2), influence the photoassociation spectrum. To answer this question, we scale the exponents in Eq. (2) by $\pm 10\%$. The resulting photoassociation spectra are also depicted in Fig. 6. If $\Gamma(R)$ is being weakened (larger α and β, red and blue lines in Fig. 6), individual rovibrational lines emerge. On the other hand, the spectrum becomes almost flat for stronger $\Gamma(R)$ (green line in Fig. 6), as expected: If the ionization probability is very high, a wave packet cannot oscillate back and forth in the potential even once, i.e., the discrete nature of the bound levels cannot be established. Thus, for a potential energy curve located at shorter inter-particle separations, the prospects for photoassociation spectroscopy depend highly on the actual strength of $\Gamma(R)$. In turn, photoassociation spectroscopy can be used to determine this strength. If the ionization probability is not too high, such that single rovibrational peaks can be resolved, the increase of peak widths with binding energy should moreover allow to determine the functional form of $\Gamma(R)$. In other words, photoassociation spectra as those represented by the blue line in Fig. 6 can be used to fully map out $\Gamma(R)$, a quantity that still poses a rather large challenge to *ab initio* calculations.

IV. CONCLUSIONS

We have studied the prospects for photoassociation as a spectroscopic tool to study Penning ionization reactions. Introducing an *ab initio* model for the simplest example, Penning ionization of metastable helium with argon, we find usability of this tool to be determined by the position of the excited state well. For a potential with a comparatively large equilibrium distance, about 10 bohr in our case, the probability of Penning ionization is larger than in the entrance channel, yet sufficiently small to allow for resolving single rovibrational levels. Photoassociation can then be observed by peaks in the ionization rate as a function of laser detuning.

In merged beams, the collision energy in the entrance channel can precisely be controlled. Choosing in this way to photoassociate out of a shape resonance allows for unequivocally

determining the rotational quantum number of the resonance since, compared to regular scattering states, a shape resonance leads to clearly enhanced photoassociation peaks in the rotational progression. While the enhancement amounts to about one order of magnitude for diffuse, above-the-barrier shape resonances, enhancements up to three orders of magnitude are expected for shape resonances whose energy is well below the top of the rotational barrier.

For a potential with a comparatively small equilibrium distance, about 5 bohr in our case, the probability of Penning ionization becomes very large. Whether photoassociation peaks as a function of laser detuning can be observed or not, then depends very sensitively on the value of the exponents in the imaginary potential. We have started our calculations with values from the literature, obtained by fitting experimental data obtained for thermal collision energies [22]. Changing these values by only -10 per cent completely washes out any remnants of a peak structure, whereas a change in +10 per cent leads to clearly observable photoassociation peaks. Photoassociation spectroscopy can thus be used to accurately gauge the exponents of the imaginary potential. Moreover, if the Penning ionization probability is sufficiently small to allow for peak widths to be determined, an increase of the peak width with binding energy, respectively laser detuning, can be used to fully map out the functional form of the imaginary potential.

In summary, we find photoassociation spectroscopy to be an extremely useful tool to obtain in-depth information on Penning ionization reactions, provided the ionization proceeds not too fast. Our conclusions should hold also for collision partners other than argon, in particular if these are closed-shell.

Acknowledgments

Financial support from the German-Israeli Foundation, grant no. 1254, is gratefully acknowledged.

---

[1] S. Y. T. van de Meerakker, H. L. Bethlem, N. Vanhaecke, and G. Meijer, Chem. Rev. **112**, 4828 (2012).

[2] L. D. van Buuren, C. Sommer, M. Motsch, S. Pohle, M. Schenk, J. Bayerl, P. W. H. Pinkse, and G. Rempe, Phys. Rev. Lett. **102**, 033001 (2009).

[3] E. Narevicius and M. G. Raizen, Chem. Rev. **112**, 4879 (2012).

[4] A. B. Henson, S. Gersten, Y. Shagam, J. Narevicius, and E. Narevicius, Science **338**, 234 (2012).

[5] E. Lavert-Ofir, Y. Shagam, A. B. Henson, S. Gersten, J. Kłos, P. S. Żuchowski, J. Narevicius, and E. Narevicius, Nature Chem. **6**, 332 (2014).

[6] B. Bertsche, J. Jankunas, and A. Osterwalder, CHIMIA **68**, 256 (2014).

[7] J. Jankunas, B. Bertsche, K. Jachymski, M. Hapka, and A. Osterwalder, J. Chem. Phys. **140**, 244302 (2014).

[8] J. Jankunas, K. S. Reisyan, and A. Osterwalder, J. Chem. Phys. **142**, 104311 (2015).

[9] Y. Shagam, A. Klein, W. Skomorowski, R. Yun, V. Averbukh, C. P. Koch, and E. Narevicius, Nat. Chem. **7**, 921 (2015).

[10] M. Hapka, G. Chałasiński, J. Kłos, and P. S. Żuchowski, J. Chem. Phys. **139**, 014307 (2013).

[11] U. Fano, Phys. Rev. **124**, 1866 (1961).

[12] H. Feshbach, Ann. Phys. **19**, 287 (1962).

[13] B. E. Londoño, J. E. Mahecha, E. Luc-Koenig, and A. Crubellier, Phys. Rev. A **82**, 012510 (2010).

[14] F. Masnou-Seeuws and P. Pillet, Adv. in At., Mol. and Opt. Phys. **47**, 53 (2001).

[15] K. M. Jones, E. Tiesinga, P. D. Lett, and P. S. Julienne, Rev. Mod. Phys. **78**, 483 (2006).

[16] C. P. Koch, R. Kosloff, E. Luc-Koenig, F. Masnou-Seeuws, and A. Crubellier, J. Phys. B **39**, S1017 (2006).

[17] C. P. Koch and M. Shapiro, Chem. Rev. **212**, 4928 (2012).

[18] J. Léonard, M. Walhout, A. P. Mosk, T. Müller, M. Leduc, and C. Cohen-Tannoudji, Phys. Rev. Lett. **91**, 073203 (2003).

[19] P. E. Siska, Rev. Mod. Phys. **65**, 337 (1993).

[20] T. H. Dunning, J. Chem. Phys. **90**, 1007 (1989).

[21] H.-J. Werner, P. J. Knowles, F. R. M. R. Lindh, M. Schütz, P. Celani, T. Korona, A. Mitrushenkov, G. Rauhut, T. B. Adler, R. D. Amos, et al., *MOLPRO, version 2010.1, a package of ab initio programs* (2010), see http://www.molpro.net.

[22] S. Burdenski, R. Feltgen, F. Lichterfeld, and H. Pauly, Chem. Phys. Lett. **78**, 296 (1981).

[23] K. Sando and A. Dalgarno, Mol. Phys. **20**, 103 (1971).

[24] R. Napolitano, J. Weiner, C. J. Williams, and P. S. Julienne, Phys. Rev. Lett. **73**, 1352 (1994).

[25] H. S. Lee, Y. S. Lee, and G.-H. Jeung, J. Phys. Chem. A **103**, 11080 (1999).

[26] R. González-Férez and C. P. Koch, Phys. Rev. A **86**, 063420 (2012).